AIAA JOURNAL
Vol. 38, No. 7, July 2000

Parametric Study of Simplex Fuel Nozzle Internal Flow and Performance

A. T. Sakman,* M. A. Jog,† and S. M. Jeng‡
University of Cincinnati, Cincinnati, Ohio 45221
and
M. A. Benjamin§
Parker Hannifin Corporation, Mentor, Ohio 44060

A numerical study is presented of the effects of changes in simplex nozzle geometry on its performance. A computational model based on the arbitrary-Lagrangian-Eulerian method with an adaptive grid-generation scheme is used. Three nondimensional geometric parameters are studied: the length-to-diameter ratio of the swirl chamber L_s/D_s and orifice l_o/d_o and the swirl-chamber-diameter-to-exit-orifice-diameter ratio D_s/d_o. The variations in the atomizer performance, caused by the changes in the geometric parameters, are presented in terms of the film thickness at the exit of the orifice, the spray cone angle, and the discharge coefficient. Results indicate that these geometric parameters have a significant effect on the internal flow and performance of simplex nozzles. With a constant mass flow through the nozzle over the range of parameters considered, an increase in L_s/D_s produces an increase in the film thickness at the orifice exit, a decrease in the spray cone half-angle, and a slight decrease followed by an increase in the discharge coefficient. Conversely, increasing l_o/d_o decreases film thickness, spray cone angle, and discharge coefficient. An increase in D_s/d_o results in a decrease in film thickness and discharge coefficient and a decrease in spray cone angle.

Nomenclature

A_o	= orifice area, m^2
A_p	= total inlet area, m^2
C_d	= discharge coefficient, $\dot{m}/[A_0\sqrt{(2\rho\Delta p)}]$
D_p	= inlet slot diameter, m
D_s	= swirl-chamber diameter, m
d_o	= exit-orifice diameter, m
K	= atomizer geometric constant, $A_p/(D_s d_o)$
L_s	= swirl-chamber length, m
l_o	= orifice length, m
m	= vertex mass
$\dot{m}$	= mass-flow rate, kg/s
p	= mean pressure, N/m^2
p_∞	= ambient pressure, N/m^2
R_1, R_2	= radii of curvature, m
r	= radial coordinate, m
t	= time, s
t_s	= film thickness, m
t_s^*	= dimensionless film thickness, $t_s/(d_o/2)$
u	= axial velocity, m/s
v	= radial velocity, m/s
w	= swirl velocity, m/s
x	= axial coordinate, m
Δp	= pressure differential, N/m^2
θ	= spray cone half-angle, deg
μ	= dynamic viscosity, kg m/s
μ_t	= turbulent dynamic viscosity, kg m/s
ρ	= fluid density, kg/m^3
σ	= surface tension, N/m

Subscript

av	= average

Superscript

*	= dimensionless quantities

Introduction

SIMPLEX nozzles (pressure-swirl atomizers) producing hollow-cone sprays are widely used in airbreathing gas turbine engines because of their good atomization characteristics and relative simplicity. Double-annular dome combustors using simplex nozzles with primary air swirlers are being used in advanced aeroengines for cleaner combustion. In a simplex nozzle the fuel is forced under high pressure to enter a swirl chamber through virtually tangential inlet slots at the outer wall, forming an air core along the centerline because of high swirl velocity. The fuel exits the nozzle through a small orifice with even higher swirl velocity that forces the liquid to disperse radially outward to form a hollow cone. The thin liquid sheet then becomes unstable and breaks up to form a spray. Because the droplet size distribution and local fuel-to-air ratios significantly affect combustion efficiency and emissions, it is important to predict the impact of atomizer geometry on these variables.

It is well established that mean droplet diameter and spray angle are the two most important parameters governing nozzle performance.[1] Many studies on fuel atomization have shown that the mean droplet size is directly related to the thickness of the liquid film emanating from the nozzle, with the mean drop diameter being roughly proportional to the square root of the film thickness.[2,3] Therefore, the film thickness is also considered as an important parameter governing nozzle performance. For a given mass-flow rate studies have shown that geometrical design of the simplex nozzle is the primary factor that determines the internal flowfield and influences the nozzle performance parameters.[1] Despite the simple geometry of the simplex nozzle, the flow phenomena within the nozzle are complex. Assuming an inviscid flow through the nozzle, Taylor[4] and Giffen and Muraszew[5] have shown that geometry effects on the characteristics of the liquid sheet emanating from the nozzle can be expressed in terms of an atomizer constant K (defined as the ratio of the total area of the inlet ports to the product of the swirl-chamber diameter and the discharge orifice diameter). However, in practice, viscous effects are present, which depend on the form and area of the wetted surface, as expressed by ratio of length

Presented as Paper 98-3906 at the AIAA/ASME/SAE/ASEE 34th Joint Propulsion Conference, Cleveland, OH, 13–15 July 1998; received 13 May 1999; revision received 5 November 1999; accepted for publication 29 November 1999.

*Research Assistant; currently Project Engineer, ACRI, 10901 Reed Hartman Highway, Suite 223, Cincinnati, OH 45242.
†Associate Professor, Department of Mechanical, Industrial, and Nuclear Engineering.
‡Associate Professor, Department of Aerospace Engineering and Engineering Mechanics.
§Technical Team Leader, Gas Turbine Fuel Systems Division.

to diameter of the swirl chamber L_s/D_s and that of the orifice l_o/d_o and ratio of swirl-chamber diameter and exit-orifice diameter D_s/d_o. Therefore, these parameters also influence the performance of simplex atomizers.[1] Elkotb et al.[6] made measurements of drop sizes with a number of simplex nozzles, keeping pressure drop across the nozzle constant. They found that with increasing L_s/D_s mean drop size first decreases then increases. The mean drop size was seen to initially increase with increasing l_o/d_o, with virtually no change beyond $l_o/d_o = 2$. Rizk and Lefebvre[7] found that the film thickness decreases with decreasing d_o, inlet port diameter, and increases with increasing D_s. Only a weak dependence of film thickness on l_o and L_s was observed with film thickness decreasing with increasing l_o and decreasing L_s. Suyari and Lefebvre[8] measured liquid-film thickness at the nozzle exit and compared their measurements with available correlations. Their measurements showed that film thickness increased with increasing atomizer constant and the experimental data were in good agreement with the predictions based on Giffen and Muraszew's analysis. Jones[9] has proposed a correlation for the discharge coefficient for large-scale nozzles, which includes the effect of nozzle geometry parameters. He found that the discharge coefficient increases with atomizer constant K, L_s/D_s, and D_s/d_o, and decreases slightly with l_o/d_o. Recent results of Benjamin et al.[10] show that these effects are sensitive to the range of parameter values considered. They have presented correlations for discharge coefficient, film thickness, and spray angle for large-scale simplex nozzles. They found that l_o/d_o has a weak influence on C_d, with a trend opposite of that reported by Jones.[9] They showed that the discharge coefficient increases with l_o/d_o, at higher values of l_o/d_o. Both the atomizer constant and D_s/d_o were shown to have a strong influence on film thickness and spray cone angle.

Only recently have computational studies of the flow in a simplex atomizer been carried out. The main difficulty in the numerical simulation of the flow in a simplex nozzle is the accurate tracking of the liquid/air interface. Yule and Chinn[11] used commercially available software (Fluent) to solve for the liquid flowfield in a simplex nozzle. They determined the position of the interface with an approximate method and restricted their simulation to laminar flow. Recently, we have developed a computational model to track accurately the liquid/air interface and predict the flow in a simplex nozzle.[12] This was accomplished by using the arbitrary-Lagrangian-Eulerian (ALE) method.[13] Our numerical model was validated by comparing computational predictions and experimental measurements of the variations of film thickness, spray cone angle, and discharge coefficient with atomizer constant, as well as the shape of the gas/liquid interface.[12] Excellent agreement between computational and experimental results was observed, thereby confirming that the ALE method can predict accurately the shape of the interface, film thickness, cone angle, and discharge coefficient. The effect of atomizer constant K on the flow in a simplex nozzle was investigated. With decreasing K the film thickness decreases, spray cone angle increases, and discharge coefficient decreases. A decrease in K can be achieved by reduction in the inlet swirl slot area. For a given mass-flow rate this causes the swirl velocity, and correspondingly the centrifugal force, to increase, thereby increasing the spray cone angle and decreasing the film thickness. In this paper we have investigated the effects of three other geometric parameters (L_s/D_s, l_o/d_o, and D_s/d_o) on the flow in a simplex nozzle. The computational model based on the ALE method is used. The variations of film thickness, spray cone angle, and discharge coefficient are obtained. The mass-flow rate through the nozzle is kept constant for all cases. We have covered a range of L_s/D_s from 0.1 to 1.5, a range of l_o/d_o from 0.2 to 2.0, and a range of D_s/d_o from 3.5 to 6.5.

Computational Model

A schematic of a typical simplex atomizer is shown in Fig. 1. The liquid fuel enters the swirl chamber and exits through the small circular orifice. Because of the high swirl velocity, the liquid is centrifuged toward the walls, and an air core is formed along the centerline of the nozzle. The computational domain is restricted to the liquid phase because shear stress acting on the gas/liquid interface is negligible because of the very small density and viscosity ratios of air to liquid investigated here. The position and shape of the interface, however, are not known a priori and must be determined as a part of

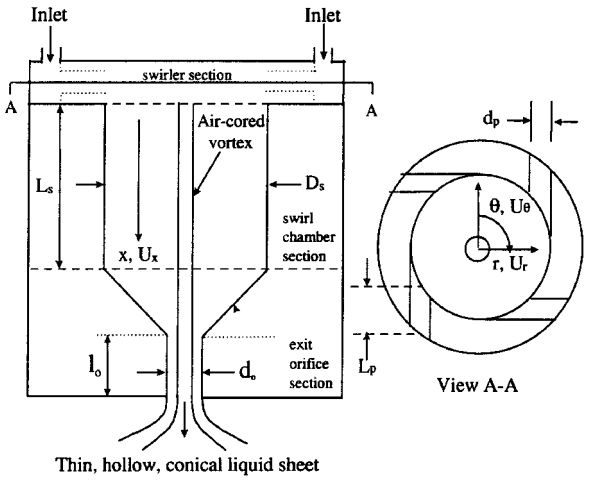

Fig. 1 Schematic of a simplex nozzle.

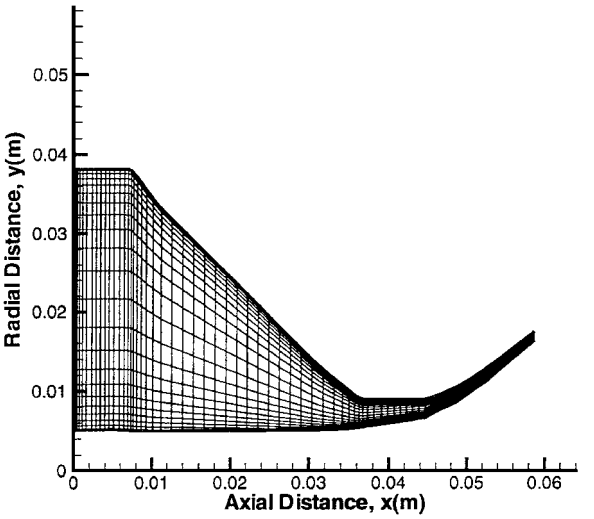

Fig. 2 Mesh plot of the computational domain.

the solution. The flowfield is considered axisymmetric and is calculated by solving the continuity and the Navier–Stokes equations. A sketch of the computational domain with the adaptive grid is shown in Fig. 2. As the flowfield is considered axisymmetric, only half of the flow cross section is shown in the figure. Also, notice the clustered grid structure in the regions where high gradients are expected.

The governing equations in cylindrical coordinates are

$$\frac{\partial u}{\partial x} + \frac{1}{r}\frac{\partial (rv)}{\partial r} = 0 \tag{1}$$

$$\rho\frac{\partial u}{\partial t} + \rho u\frac{\partial u}{\partial x} + \frac{\rho v}{r}\frac{\partial u}{\partial r} = -\frac{\partial p}{\partial x} + (\mu + \mu_t)\left(\frac{\partial^2 u}{\partial x^2} + \frac{1}{r}\frac{\partial}{\partial r}\left(r\frac{\partial u}{\partial r}\right)\right) \tag{2}$$

$$\rho\frac{\partial v}{\partial t} + \rho u\frac{\partial v}{\partial x} + \frac{\rho v}{r}\frac{\partial v}{\partial r} = -\frac{\partial p}{\partial r} + (\mu + \mu_t)\left(\frac{\partial^2 v}{\partial x^2} + \frac{1}{r}\frac{\partial}{\partial r}\left(r\frac{\partial v}{\partial r}\right)\right) + \frac{\rho w^2}{r} - 2(\mu + \mu_t)\frac{v}{r} \tag{3}$$

$$\rho\frac{\partial w}{\partial t} + \rho u\frac{\partial w}{\partial x} + \frac{\rho v}{r}\frac{\partial w}{\partial r} = (\mu + \mu_t)\left(\frac{\partial^2 w}{\partial x^2} + \frac{1}{r}\frac{\partial}{\partial r}\left(r\frac{\partial w}{\partial r}\right)\right) - \frac{\rho v w}{r} \tag{4}$$

Here μ_t is the eddy viscosity coefficient determined by using the Baldwin–Lomax model.[14] The no-slip condition is specified at the solid boundaries, and the radial and angular velocities are specified at the annular inlet slot. The flow properties at the end of the liquid

are extrapolated from interior grid points. At the liquid/air interface the normal stress balance is $p = p_\infty + \sigma(1/R_1 + 1/R_2)$, where p_∞ is assumed to be constant.

The governing equations and boundary conditions are discretized in a finite volume fashion. A staggered grid structure is used for pressure and velocity cells. The ALE method is used with an adaptive grid technique to track the moving interface. The ALE method[13] is divided into two stages. In the fully Lagrangian stage of the ALE method, the cells move with the same velocity as that of the fluid, and there is no mass interchange between the cells. A predictor–corrector method is used to solve the governing equations. The predictor first determines the temporary velocity increment for node (i, j) for each time step based on a temporary new pressure field p^*. The velocity increment is calculated as

$$\Delta V_{i,j} = \frac{\Delta t}{m_{i,j}} \oint_s p^* \, dA \tag{5}$$

where s is the surface area of the momentum cell, $m_{i,j}$ is the cell mass, and Δt is the time step. The velocities and positions of the nodes are updated as

$$V^*_{i,j} = V^N_{i,j} + \Delta V_{i,j} \tag{6}$$

$$X^*_{i,j} = X^N_{i,j} + V^*_{i,j} \Delta t \tag{7}$$

The updated cell mass is then calculated based on the temporary volume. If the updated mass does not match with the mass of the preceding time step, then the corrector step uses the conjugate-gradient method to find a new pressure field. The position, velocity, and pressure values are set when the cell mass converges. The solution was considered to be converged if the maximum relative error in cell mass between two iterations was less than 10^{-7}.

In the second stage of the ALE method, a new grid is generated adaptively to the new interface. Mass and momentum fluxes caused by moving the cells from their Lagrangian positions to their positions in the new grid are calculated using a donor–acceptor method. Then the velocity components at the new grid points are calculated for the new time. The free surface position moves toward its steady-state position with each computational time step. Steady state is reached when the normal velocity component at the interface diminishes to zero.

The computational results were obtained with a grid of 91 points in the axial direction and 41 points in the radial direction. To test grid independence of the solutions, results for two cases (with the maximum and the minimum values of the atomizer constant) were calculated by doubling the number of grid points in both directions. The results for film thickness, spray cone angle, and the discharge coefficient were essentially unchanged (< 1%). With a change in the number of grid points from 91 × 41 to 181 × 81, for $K = 0.17$ and 0.3, dimensionless film thickness, spray cone half-angle, and discharge coefficient changed from 0.237, 44.26, 0.182 to 0.234, 44.32, 0.184 and from 0.273, 38.66, 0.243 to 0.272, 38.68, 0.244, respectively.

Model Validation

Experimental measurements of internal flowfield, film thickness, and cone angle were carried out to validate the computational model. A large-scale prototype nozzle (exit-orifice diameter of 18 mm) was used in the experiments as detailed measurements of the internal flowfield are practically impossible on small-scale nozzles (exit-orifice diameter ~1 mm) typically used in aircraft engines. Water was used as the working fluid in the experiments. The computational model assumes the flow to be axisymmetric. This assumption requires determination of an equivalent annular inlet slot instead of the finite number of slots present in the real nozzle. The width of the annular slot as well as the radial and tangential velocities at the inlet are calculated by matching the angular momentum, total mass-flow rate, and the kinetic energy of the liquid at the inlet ports with those of the experiments. The body of the nozzle is made of optical quality plexiglass, and the velocity measurements were made by a particle image velocimetry (PIV) technique. The illuminated PIV probe is provided by a 6-W coherent argon-ion laser. The laser beam passes through a mechanical chopper operated at 2000 Hz. This chopped light train is then guided through several mirrors and a laser sheet

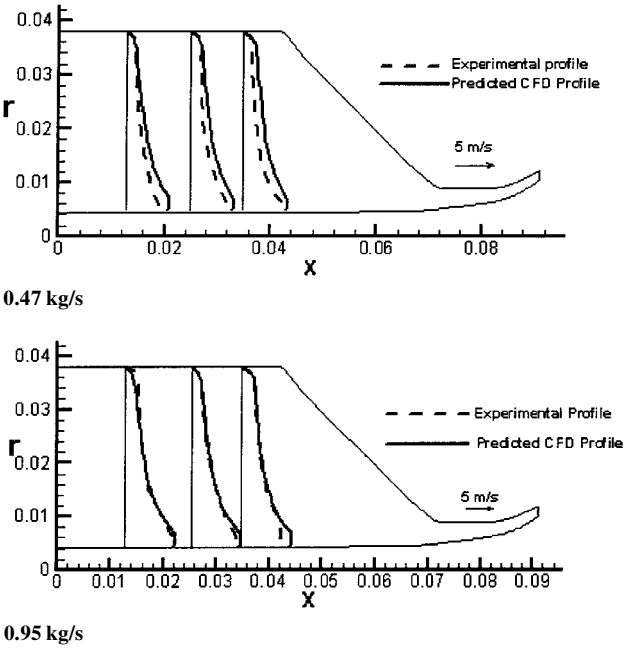

Fig. 3 Comparison of swirl velocity profiles at three different cross sections of the swirl chamber.

generator, which produces a horizontal sheet of 100 mm in width and 1 mm thickness, and then passes through the nozzle for PIV measurements. Silver-coated seeding particles (approximately 11 μm in mean diameter with specific gravity of 1.26) are injected into the large-scale nozzle. The PIV images are taken at 1/500 s shutter speed. Four images for each seeding particle are obtained in each photograph. The velocities are then determined by image processing. The details of the experimental setup and technique are available in Holtzclaw et al.[15]

Figure 3 shows a comparison of swirl velocity measurements and predictions at several axial locations along the nozzle, with mass-flow rates of 0.47 and 0.95 kg/s [7.5 gal/min (GPM) and 15 GPM], respectively. For a 0.47 kg/s flow rate the computational predictions are slightly higher than the measurements, whereas for a 0.95 kg/s flow rate the two are practically indistinguishable. The difference between the computational and experimental results at the lower flow rate can be attributed to uncertainty in mass-flow rate determination in the experiments. Also, as mentioned earlier, detailed comparisons of computational predictions and experimental measurements of the variations of film thickness, spray cone angle, and discharge coefficient with atomizer constant, as well as the shape of the gas/liquid interface, were reported in Jeng et al.[12] The computational predictions were seen to agree well with the measurements, thereby validating the numerical model. The dimensionless flow parameter that governs the flow phenomena in the nozzle is the Reynolds number.[16] The range of the Reynolds number based on the average axial velocity at the nozzle exit and the exit diameter was 2.7×10^5 to 4×10^5 in the large-scale experiments. This is similar to the range of the Reynolds number encountered in small-scale practical nozzles. Therefore, the preceding agreements validate the computational model at both large and small scale.

Results and Discussion

The validated computational model is used to investigate the effects of nozzle geometric parameters on the flow and performance. While studying the effects of changes in L_s/D_s, only L_s is varied, whereas all other dimensions are kept constant. Similarly, l_o and D_s are varied to change l_o/d_o and D_s/d_o, respectively. Although the other two parameters remain unchanged when L_s/D_s or l_o/d_o are varied, both L_s/D_s and the atomizer constant K $[= A_P/(D_s d_o)]$ change with changing D_s in D_s/d_o. Therefore, to isolate the effects of D_s/d_o, L_s and A_P are varied such that K and L_s/D_s remain constant while changing D_s in D_s/d_o. When one parameter was changed, other parameters were kept constant at $L_s/D_s = 1$, $l_o/d_o = 0.5$, and $D_s/d_o = 4.22$. The angle of the tapered section

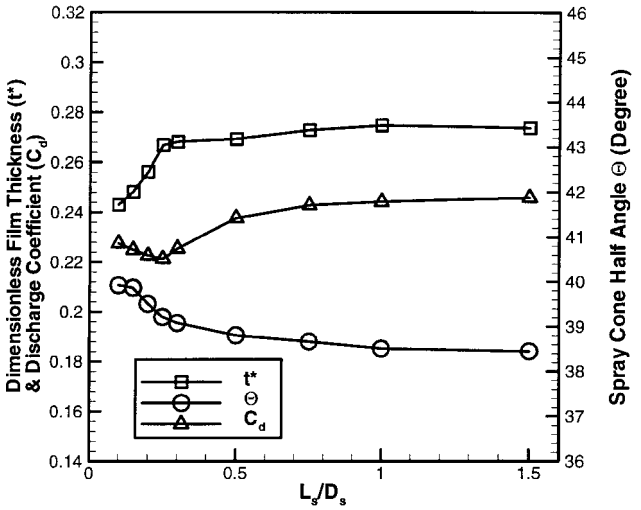

Fig. 4 Variation of film thickness at the exit, spray cone half-angle, and discharge coefficient with L_s/D_s.

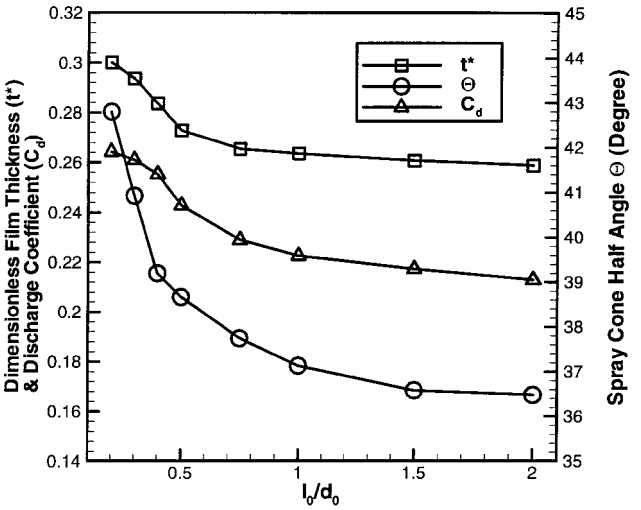

Fig. 5 Variation of film thickness at the exit, spray cone half-angle, and discharge coefficient with l_o/d_o.

connecting the swirl chamber to the exit orifice was 45 deg for all cases studied. For each case the variation in the film thickness at exit, the spray cone half-angle, and the discharge coefficient are reported. The results are obtained with a constant mass-flow rate through the nozzle. In many experimental studies available in the literature, measurements of film thickness and spray angle have been carried out with a constant pressure drop across the nozzle. The variations in the nozzle performance parameters obtained with a constant mass-flow rate are likely to be different from those obtained with a constant pressure drop across the nozzle.

Effect of L_s/D_s

The variations of film thickness (made dimensionless by exit-orifice radius), discharge coefficient, and spray cone half-angle with L_s/D_s are shown in Fig. 4. There is a limit on the minimum value that L_s/D_s can take because L_s geometrically cannot be less than the width of the annular inlet slot. Figure 4 shows that starting from an L_s/D_s of 0.1, up to 0.25, there is a steep increase in the thickness, while the trend diminishes beyond that point. The discharge coefficient, which is inversely proportional to the square root of the pressure drop, is seen to first slightly decrease then increase with L_s/D_s. For a given swirl-chamber diameter, with larger swirl-chamber length, the frictional losses in the nozzle increase. This reduces the swirl in the swirl chamber and the exit orifice and increases the film thickness. Because the mass-flow rate is kept constant throughout the study, from conservation of mass, we have

$$\dot{m} = \rho u_{\text{av}} \pi \left\{ (d_o/2)^2 - [(d_o/2) - t_s]^2 \right\} \tag{8}$$

Therefore, for a given mass flow the average axial velocity u_{av} decreases as the film thickness increases. With the increasing flow cross-sectional area at the exit caused by the increased thickness and reduced axial velocity, the discharge coefficient increases. The behaviors of increase in film thickness and discharge coefficient with increasing L_s are consistent with the trends reported by Rizk and Lefebvre[7] and by Jones.[9] The increase in L_s appears to have a stronger influence on the swirl velocity compared to that on the axial velocity. The average swirl velocity decreases faster than the average axial velocity, and as expected, this decrease in the swirl velocity component leads to a reduction in the spray cone angle. It is evident from these results that the effect of change in L_s/D_s on the performance variables is more significant at lower L_s/D_s, whereas it diminishes at $L_s/D_s > 1$.

Effect of l_o/d_o

Figure 5 shows the variations of dimensionless film thickness ($t_s^* = 2t_s/d_o$), discharge coefficient, and spray cone half-angle with l_o/d_o. The figure shows that the film thickness decreases with increasing l_o/d_o. This trend of increase in film thickness with exit-orifice length is opposite of that obtained by Rizk and Lefebvre.[7] The difference in results presented here and those in Ref. 7 is caused by the different boundary conditions (constant mass flow vs constant pressure drop) in the two studies. For a given l_o the value of l_o/d_o increases with decreasing d_o. Therefore, for a large l_o/d_o nozzle, to maintain the same mass flow as a small l_o/d_o nozzle the fluid has to be squeezed through a long narrow orifice requiring a much larger pressure differential across the nozzle. This increased pressure leads to higher axial velocities and lower film thickness at exit. Conversely, if the pressure drop across the nozzle is kept constant, the mass-flow rate will decrease with increasing l_o/d_o, resulting in lower axial velocity and higher film thickness. Therefore the behavior of film thickness with exit-orifice length observed here and in Ref. 7 is consistent with the respective boundary conditions. Similar to the variation of thickness with L_s/D_s, the trend is rather steep at lower l_o/d_o, whereas its gradient decreases at higher l_o/d_o. As the pressure drop across the nozzle increases with increasing l_o/d_o, there is a reduction in the discharge coefficient with increasing l_o/d_o. This behavior is similar to the trend observed by Jones[9]; however, the effect is somewhat larger, indicating that l_o/d_o is an important parameter in determining the pressure drop across the nozzle.

The principle of conservation of mass dictates that the variation of the average axial velocity at exit must have a trend opposite to that of the film thickness. Therefore, the axial velocity increases with l_o/d_o. The swirl velocity on the other hand has a less steep variation compared with u_{av}, which causes a decrease in $w_{\text{av}}/u_{\text{av}}$. As the ratio of the average swirl to axial velocity at exit is the primary parameter that determines the spray cone angle, a decrease in $w_{\text{av}}/u_{\text{av}}$ leads to smaller spray cone half-angle.

Effect of D_s/d_o

The variations of dimensionless film thickness, spray cone half-angle, and discharge coefficient with changing D_s/d_o are shown in Fig. 6. As D_s/d_o is increased, the fluid is being squeezed through a narrower orifice compared to the swirl chamber. This flow situation is similar to a sudden contraction in a pipe flow, where the pressure drop increases significantly as the contraction ratio is increased. This increase in pressure drop across the nozzle results in a reduction in the discharge coefficient. With a constant mass flow across the nozzle, the increase in the applied pressure leads to an increase in the axial velocity and the film thickness that the nozzle exit decreases. In this case both the swirl and the axial velocities increase with D_s/d_o. However, their relative change leads to the ratio of the swirl and axial velocity to decrease, and the variation of spray cone angle follows the behavior of the ratio of swirl to axial velocity and decreases with increasing D_s/d_o. The difference in the increase in swirl and axial velocities is likely to be caused by the nature of flow distribution in the nozzle. Holtzclaw et al.[15] have shown that in the swirl chamber large axial velocities are confined to a region close to the liquid/air interface, whereas the swirl velocity is significant in the entire cross section of the swirl chamber as shown in Fig. 3.

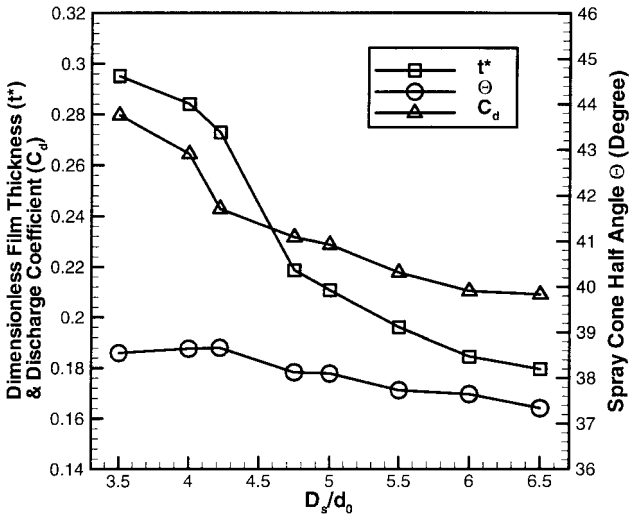

Fig. 6 Variation of film thickness at the exit, spray cone half-angle, and discharge coefficient with D_s/d_o.

Therefore a change in D_s has a smaller effect on the axial velocity distribution compared with that on the swirl velocity distribution. Hence to maintain a constant mass flow, an increase in the applied pressure across nozzle with high D_s/d_o causes the axial velocity to increase more significantly than the swirl velocity.

Conclusions

A computational parametric study of the internal flow and performance of a simplex nozzle has been carried out. For constant mass-flow rate the effects of three geometric parameters (L_s/D_s, l_o/d_o, and D_s/d_o) on simplex nozzle performance were investigated. For the range of parameters considered here, D_s/d_o appears to have the most influence on the performance variables studied. An increase in D_s/d_o results in a decrease in the film thickness at the exit and an increase in the pressure drop in the nozzle, giving a monotonous decrease in the discharge coefficient. The spray cone half-angle also decreases with increasing D_s/d_o.

The effects of an increase in L_s/D_s are a larger film thickness at the exit, lower average axial and swirl velocities at the exit, a slight decrease followed by an increase in the discharge coefficient, and a decrease in the spray cone half-angle. When changing L_s/D_s, the pressure drop changed by only 20% and the spray cone half-angle by only 3%.

As is the case for L_s/D_s, the effects of l_o/d_o on the studied variables are more pronounced at low l_o/d_o, whereas the trends become more gradual as l_o/d_o increases. The effects of an increase in l_o/d_o are a decrease in film thickness at the exit, an increase in average axial and swirl velocities at the exit, a significant decrease in the discharge coefficient, and a decrease in the spray cone half-angle. The overall effect of the change in l_o/d_o is larger than that of L_s/D_s.

Acknowledgments

This work was supported by the Parker Hannifin Corporation and by NASA John H. Glenn Research Center at Lewis Field under Grant NAG3-1987. We would like to thank J. Xue for his help in preparing some of the figures.

References

[1]Lefebvre, A. H., *Atomization and Sprays*, Hemisphere, New York, 1989, pp. 204–222 and 281–289.

[2]Dombrowski, N., and Johns, W. R., "The Aerodynamic Instability and Disintegration of Viscous Liquid Sheets," *Chemical Engineering Science*, Vol. 18, 1963, pp. 203–214.

[3]Wang, X. F., and Lefebvre, A. H., "Mean Drop Sizes from Pressure Swirl Nozzles," *Journal of Propulsion and Power*, Vol. 3, No. 1, 1987, pp. 11–18.

[4]Taylor, G. I., "The Mechanics of Swirl Atomizers," *Seventh International Congress of Applied Mechanics*, Vol. 2, Pt. 1, 1948, pp. 280–285.

[5]Giffen, E., and Muraszew, A., *The Atomization of Liquid Fuels*, Chapman and Hall, Ltd., London, 1953, pp. 100–116.

[6]Elkotb, M. M., Rafat, N. M., and Hanna, M. A., "The Influence of Swirl Atomizer Geometry on the Atomization Performance," *Proceedings of the International Conference on Liquid Atomization Systems*, Inst. for Liquid Atomization and Spray Systems, Irvine, CA, 1978, pp. 109–115.

[7]Rizk, N. K., and Lefebvre, A. H., "Internal Flow Characteristics of Simplex Swirl Atomizers," *Journal of Propulsion and Power*, Vol. 1, No. 3, 1985, pp. 193–199.

[8]Suyari, M., and Lefebvre, A. H., "Film Thickness Measurements in a Simplex Swirl Atomizer," *Journal of Propulsion and Power*, Vol. 2, No. 6, 1986, pp. 528–533.

[9]Jones, A. R., "Design Optimization of Large Pressure-Jet Atomizers for Power Plants," *Proceedings of the Second International Conference on Liquid Atomization and Spray Systems*, Inst. for Liquid Atomization and Spray Systems, Irvine, CA, 1982, pp. 181–185.

[10]Benjamin, M. A., Mansour, A., Samant, U. G., Jha, S., Liao, Y., Harris, T., and Jeng, S. M., "Film Thickness, Droplet Size Measurements and Correlations for Large Pressure-Swirl Atomizers," American Society of Mechanical Engineers, Paper 98-GT-537, June 1998.

[11]Yule, A. J., and Chinn, J. J., "Pressure Swirl Atomizer Internal Flow and Performance," *Proceedings of the 10th Annual Conference on Liquid Atomization and Spray Systems: ILASS—Americas 1997*, Inst. for Liquid Atomization and Spray Systems, Irvine, CA, 1997, pp. 205–209.

[12]Jeng, S. M., Jog, M. A., and Benjamin, M. A., "Computational and Experimental Study of Liquid Sheet Emanating from Simplex Fuel Nozzle," *AIAA Journal*, Vol. 36, No. 2, 1998, pp. 201–207.

[13]Hirt, C. W., Amsden, A. A., and Cook, J. L., "An Arbitrary-Lagrangian-Eulerian Computing Method for All Flow Speeds," *Journal of Computational Physics*, Vol. 14, 1974, pp. 227–253.

[14]Baldwin, B., and Lomax, H., "Thin Layer Approximation and Algebraic Model for Separated Turbulent Flow," AIAA Paper 78-0257, 1978.

[15]Holtzclaw, D., Sakman, T., Jeng, S. M., Jog, M. A., and Benjamin, M. A., "Investigation of Flow in a Simplex Nozzle," AIAA Paper 97-2970, July 1997.

[16]Radcliffe, A., "The Performance of a Type of Swirl Atomizer," *Proceedings, Institution of Mechanical Engineers*, Vol. 169, 1955, pp. 93–106.

J. P. Gore
Associate Editor